the electron-transfer mechanism presented in Scheme II for $(Cp)Ti(C_8H_8)$. In the presence of TBAP, two species are present in solution, $(Cp)Ti(C_8H_8)$ and the perchlorate adduct $[(Cp)Ti(C_8H_8)ClO_4]^-$. Waves 5 and 7 are assigned to the reversible electron transfer of the perchlorate adduct, while wave 6 is assigned to the oxidation of $(Cp)Ti(C_8H_8)$. The electrochemical properties of waves 5 and 6 suggest that observation of the perchlorate adduct on the first scan (wave 5) is due to the application of the potential and does not reflect bulk solution concentrations. In the absence of perchlorate anion, the reversible oxidation of either $(Cp)Ti(C_8H_8)$ or $(Cp^*)Ti(C_8H_8)$ is found.

It is interesting that $(Cp)Ti(C_8H_8)$ in CH_3CN/TBAP does not show the presence of two species. This could be due to a significant change in the chemical reaction kinetics, but we think it is evidence of coordination of $(Cp)Ti(C_8H_8)$ by acetonitrile.

The oxidation product in the presence of perchlorate is assigned as $(\eta^5\text{-}Cp)Ti(\eta^6\text{-}C_8H_8)(ClO_4)$, since the second and all subsequent scans in the cyclic voltammogram show only waves 5 and 7. The agreement between the electronic spectra of the bulk electrolysis product and the spectroelectrochemical data suggest that this species is relatively stable. The equivalence of the protons on the NMR time scale neither supports nor negates this assignment.[2,3,8,9]

The results from MO calculations[4,5] and ESR,[8] ENDOR,[9] and photoelectron studies[11] all indicate the location of the unpaired electron in the C_8H_8 adducts is the a_1 orbital, which is primarily metal dz^2 character. The spectroelectrochemical data are consistent with these results in that the spectral changes indicate only a small perturbation of the ligand $\pi \rightarrow \pi^*$ absorption band.

Discussion

The spectroelectrochemical data provide information on the nature of the electrogenerated species, including insight into the electronic structure. However, the data for this set of complexes and for $(Cp)_2Ti(bpy)$[14] suggest that *assignment* of the site of electron transfer by spectroelectrochemical methods for organometallic species is not reliable. This is the case for (at least) two reasons. The first is that the chemical reactions that follow electron transfer typically result in significant changes in the electronic absorption spectra of the complexes and a separation of the effects due to the electron transfer and the chemical reaction is then required. The second reason is that the HOMO and LUMO cannot reliably be described as either ligand or metal centered. For example, the HOMO of $(Cp)Ti(C_7H_7)$ contains approximately 60% C_7H_7 character and 40% metal character,[6] while the HOMO of $(Cp)Ti(C_8H_8)$ is nearly 100% metal character.[4,5]

The large effect of the change from L = C_7H_7 to L = C_8H_8 on the electrochemical results is consistent with the electron-donating abilities of the respective ligands. The formal charge on the C_8H_8 ring is −2 and is +1 for C_7H_7. Hence, the observation of reduction processes for the 16-electron $(Cp)Ti(C_7H_7)$ or $(Cp^*)Ti(C_7H_7)$ species reflects the decrease in electron density on the complexes. The easy oxidation of the 17-electron $(Cp)Ti(C_8H_8)$ or $(Cp^*)Ti(C_8H_8)$ and the lack of observation of a reduction process is also consistent. However, it should be pointed out that MO calculations for both of these species result in a charge on the rings that is significantly different from the formal charge.[4-6] The difference between the oxidation potentials for the cyclooctatetraene adducts and the tropylium ion adducts is approximately 1 V. If one assumes that the energy difference between the HOMO and the LUMO is approximately the same for these species, then one would predict a reduction potential for the cyclooctatetraene adducts to be near 3.0 V vs SCE.

Acknowledgment is made by J.E.A. to the donors of the Petroleum Research Fund, administered by the American Chemical Society, for the support of this research.

Registry No. $(Cp)Ti(C_7H_7)$, 51203-49-7; $(Cp)Ti(C_7H_7)^-$, 115338-78-8; $(Cp)Ti(C_7H_7)^+$, 132854-60-5; $(Cp^*)Ti(C_7H_7)$, 104453-33-0; $[(Cp^*)Ti(C_7H_7)]^-$, 132774-48-2; $[(Cp^*)Ti(C_7H_7)]^+$, 132774-49-3; $(Cp)Ti(C_8H_8)$, 11065-40-0; $[(Cp)Ti(C_8H_8)]$, 57208-15-8; $(Cp^*)Ti(C_8H_8)$, 104469-59-2; $[(Cp^*)Ti(C_8H_8)]^+$, 132774-50-6; $[(Cp^*)Ti(C_8H_8)]ClO_4$, 132774-51-7; TBAP, 1923-70-2; $TBA(BF_4)$, 429-42-5; THF, 109-99-9; CH_3CN, 75-05-8; CH_2Cl_2, 75-09-2.

Molecular Self-Recognition and Crystal Building in Transition-Metal Carbonyl Clusters: The Cases of $Ru_3(CO)_{12}$ and $Fe_3(CO)_{12}$

Dario Braga* and Fabrizia Grepioni

Dipartimento di Chimica "G. Ciamician", Università di Bologna, Via Selmi 2, 40126 Bologna, Italy

Received June 22, 1990

The construction of the organometallic crystals of $Ru_3(CO)_{12}$ and $Fe_3(CO)_{12}$ has been investigated by means of potential energy calculations and computer graphic analysis. It has been found that the crystallization process is based on the recognition of some simple packing motifs over the molecular surface that depend on the shape of the carbonyl coverage. The crystals of $Ru_3(CO)_{12}$ and $Fe_3(CO)_{12}$ are constructed via the interlocking of tetra-, tri-, and dicarbonyl units of independent molecules. New insights in the disorder of $Fe_3(CO)_{12}$ have been gained.

Introduction

The fundamental contribution made by X-ray crystallography to the understanding of chemical properties of organometallic compounds is evidenced by the large number of crystal structures reported to date. It has been less appreciated, however, that these diffraction studies also provide basic information about the molecular organization within the crystal lattice, on the intermolecular forces, and on the influence that these intermolecular forces have on the structural features. It would appear that most chemists (and crystallographers) are accustomed to regarding a *molecular* structure as the ultimate result of a *crystal*

0276-7333/91/2310-1254$02.50/0

structure analysis, thus forgetting that intermolecular interactions may be responsible for many features of the molecular structure. In an attempt to broaden this perspective we recently began an investigation into the packing modes of neutral organometallic molecules.[1] We now wish to extend this approach to the study of some low-nuclearity carbonyl clusters, focusing our attention on the relationship between the ligand distribution over the cluster surface and the molecular distribution within the lattice.

The gross external shape of a polynuclear carbonyl cluster is that of a "lumpy" object with the O atoms protruding from the surface. This molecular shape is characterized by the presence of bumps (the O atoms) and cavities (the space in between), which can be used for intermolecular locking and molecular self-assembling during the crystallization process. Although molecular *shape* and molecular *geometry* are strictly related, it is important to recognize that different distributions of bonding and nonbonding interactions (i.e. different molecular geometries) can correspond to very similar molecular shapes. Thus, for example, both $Fe_3(CO)_{12}$ and $Co_4(CO)_{12}$ possess the same shape (viz. icosahedral) but quite different structures, while $Co_2(CO)_8$ and $Fe_2(CO)_9$, in spite of the structural differences, pack in the same way in their crystals.[1] The very concept of a ligand envelope or outer ligand polyhedron, widely used to interpret the dynamic behavior of many carbonyl clusters both in solution and the solid state,[2] is essentially the recognition that a certain ligand distribution over the cluster surface is compatible with different orientations of the inner metal frame, i.e. with different molecular geometries. For the purposes of this study, we can regard the molecular geometry more as an "internal" property only partly reflected on the outer shape of the molecule.

Along this line of thinking, the recognition of particular, recurring elements of a regular molecular shape and the understanding of the way in which such elements can interact are expected to give us some hints regarding the existence of *transferable* packing motifs to be used in the understanding of the crystal packing of other molecules. We have chosen to study $Ru_3(CO)_{12}$[3] and $Fe_3(CO)_{12}$[4] because they possess two "prototypical" molecular shapes determined by the well-known anticuboctahedral and icosahedral distribution of ligands.

In order to decode the molecular self-recognition process, which is the basis of the crystallization process, we have chosen to investigate first what a single molecule (the reference molecule, RM hereafter) "sees" around itself within the crystal packing and then to reconstruct the same crystal packing by allowing the surrounding molecules, one after the other, to cling to the RM.

Our approach to crystal packing is not conventional: we confine our attention to the number and distribution of the first neighboring molecules around the RM (those constituting the "enclosure shell", ES hereafter), thus neglecting, in a sense, the full translational symmetry of the crystal lattice. The ES features are easily accessible from potential energy calculations based on the atom–atom approach. This method has already proved useful in our earlier studies of the factors controlling the crystal packing of first-row transition-metal binary carbonyls,[1] as well as in the investigation of some solid-state dynamic processes involving mononuclear, dinuclear, and polynuclear complexes.[5] Potential energy calculations within the atom–atom pairwise approach have been widely used and thoroughly tested in the field of solid-state organic chemistry.[6,7] A brief description of the method is given in the following section.

Table I. Parameters for the Atom–Atom Potential Energy Calculations[a]

	A, kcal mol^{-1}	B, Å^{-1}	C, kcal mol^{-1} Å^6
C···C	71 600	3.68	421.0
O···O	77 700	4.18	259.4
Fe···Fe[b]	270 600	3.28	3628.0
Ru···Ru[b]	372 900	3.03	8373.0

[a] For crossed interactions: $A = (A_xA_y)^{1/2}$, $B = (B_x + B_y)/2$, $C = (C_xC_y)^{1/2}$. [b] Fe···Fe and Ru···Ru interactions were treated as Kr···Kr and Xe···Xe interactions, respectively (see text).

Methodology

Packing Potential Energy Calculations. The packing potential energy (ppe) of a neutral organometallic crystal can be evaluated within the atom–atom pairwise potential energy method[6] by means of the expression

$$\text{ppe} = \sum_i \sum_j [A \exp(-Br_{ij}) - Cr_{ij}^{-6}]$$

where r_{ij} represents the nonbonded atom–atom intermolecular distance. Index i in the summation runs over all atoms of one molecule (chosen as the reference molecule, RM), and index j over the atoms of the surrounding molecules distributed according to crystal symmetry. A cutoff at 15 Å has been adopted in our calculations. The values of the coefficients A, B, and C used in this work are listed in Table I.[8] The Fe and Ru atoms, for which such coefficients are not available, are treated as the corresponding noble gases (Kr and Xe). We have found that this choice of potential coefficients performs well when dealing with mononuclear or polynuclear organometallic complexes containing only O, C, and H atoms besides the metal ones. Ionic contributions are not considered. This assumption is justified by considering that the charges on the metal atoms are small (formally zero in polynuclear compounds of the kind discussed herein) and very much shielded from the surroundings by the ligand coverage. Furthermore, the fact that these complexes are approximately spherical means that the charge will be quite uniformly distributed and therefore at any point sufficiently small to ignore, at least to a first approximation (see also ref 1 for a discussion of the coulombic terms in binary metal carbonyls).

The results of ppe calculations are used to investigate the molecular packing arrangement around the reference molecule (RM). First, the separate contributions to ppe

(1) Braga, D.; Grepioni, F.; Sabatino, P. *J. Chem. Soc., Dalton Trans.* **1990**, 3137.
(2) Benfield, R. E.; Johnson, B. F. G. *J. Chem. Soc., Dalton Trans.* **1980**, 1743. Johnson, B. F. G.; Benfield, R. E. *Inorg. Organomet. Stereochem.* **1981**, *12*, 253. Anson, C. E.; Benfield, R. E.; Bott, A. W.; Johnson, B. F. G.; Braga, D.; Marseglia, E. A.; *J. Chem. Soc., Chem. Commun.* **1988**, 889.
(3) Churchill, M. R.; Hollander, F. J.; Hutchinson, J. P. *Inorg. Chem.* **1977**, *16*, 2655.
(4) (a) Wei, C. H.; Dahl, L. F. *J. Am. Chem. Soc.* **1969**, *91*, 1351. (b) Cotton, F. A.; Troup, J. M. *J. Am. Chem. Soc.* **1974**, *96*, 4155.
(5) (a) Braga, D.; Gradella, C.; Grepioni, F. *J. Chem. Soc., Dalton Trans.* **1989**, 1721. (b) Braga, D.; Grepioni, F.; *Polyhedron* **1990**, *1*, 53. (c) Braga, D.; Grepioni, F.; Johnson, B. F. G.; Lewis, J.; Martinelli, M. *J. Chem. Soc., Dalton Trans.* **1990**, 1847.
(6) (a) Pertsin, A. J.; Kitaigorodsky, A. I. *The Atom-Atom Potential Method*; Springer-Verlag: Berlin, 1987. (b) Gavezzotti, A.; Simonetta, M. *Organic Solid State Chemistry*; Desiraju, G. R., Ed.; Elsevier: Amsterdam, 1987.
(7) Kitaigorodsky, A. I. *Molecular Crystal and Molecules*; Academic Press: New York, 1973.
(8) (a) Gavezzotti, A. *Nouv. J. Chim.* **1982**, *6*, 443. (b) Mirsky, K. *Computing in Crystallography, Proceedings of the International Summer School on Crystallographic Computing*; Delft University Press: Twente, The Netherlands; 1978; p 169. (c) Gavezzotti, A.; Simonetta, M. *Chem. Rev.* **1982**, *82*, 1.

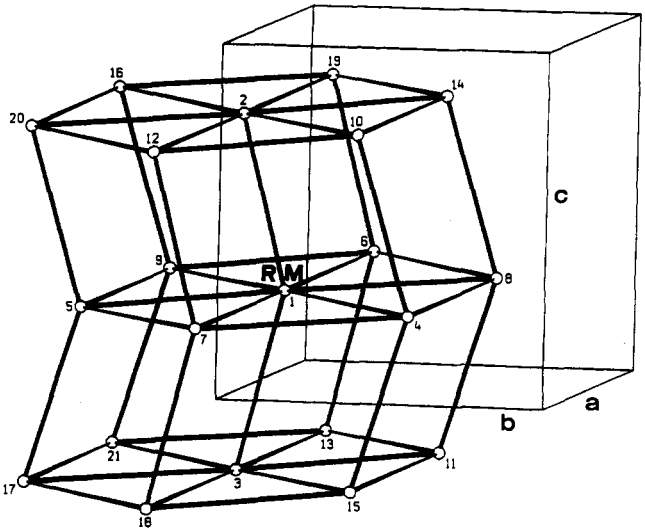

Figure 1. Schematic representation of the hexagonal layer stacking sequence characteristic of $Ru_3(CO)_{12}$ packing. The unit cell orientation is also shown. Numbers refer to the symmetry operations that generate the packing from the RM. (Symmetry operations and corresponding energy contributions to ppe are available as supplementary material.)

of all the molecules (usually in number from 60 to 80), generated around the RM by space group symmetry within the cutoff distance of 15 Å, are calculated. Then the first-neighboring molecules (those constituting the enclosure shell, ES) are selected among the surrounding molecules on the basis of the highest contributions to ppe. We have found that the ES molecules account for most of the total ppe (90–95%). It should be stressed, however, that the pairwise potential energy method is used herein *only* as a means to investigate the spatial distribution of the molecules around the one chosen as the reference, with no pretentions of obtaining "true" crystal potential energy values. On these premises, the following discussion on the various contributions to ppe will be meaningful only on a relative basis.

Details of the application of the method to organometallic crystals are given in refs 1 and 5. All calculations were carried out with the aid of the computer program OPEC.[9] SCHAKAL88[10] was used for the graphical representation of the results.

Results and Discussion

Crystal Packing in $Ru_3(CO)_{12}$. The distribution of the first-neighboring molecules in $Ru_3(CO)_{12}$ crystals is shown in Figure 1, together with the unit cell orientation (the symmetry operations that generate the packing from the RM and the individual contributions to ppe of each ES molecule are reported as supplementary material). The ES consists of 20 molecules arranged, together with the RM, in an ABA stacking sequence of parallel hexagonal layers. If the potential energy experienced by the RM (molecule 1 in Figure 1) is partitioned among the ES molecules, we find that (i) molecules 2 and 3 (those molecules approximately above and below molecule 1) give the highest contributions (−8.0 and −7.3 kcal mol^{-1}, respectively), (ii) the molecules within the central layer (molecules 4–9) contribute from −5.3 to −6.7 kcal mol^{-1}, accounting for 53% of the total ppe; (iii) the remaining molecules of the outer layers contribute less (from −0.1 to −3.4 kcal mol^{-1}) (note that a comparison of the distances between molecular centers gives the same ranking, e.g. the closer the molecules to the RM, the higher the contribution to ppe), and (iv) the ES molecules altogether account for 98% of the total ppe. It is interesting to observe that the approximately spherical $Ru_3(CO)_{12}$ does not adopt in its packing either of the close-packed distributions [hexagonal close-packed (hcp) or cubic close-packed (ccp) with an ES of 12 molecules] seen for the first-row carbonyls and commonly found in organic solids.[7] We will demonstrate in the following that this "anomalous" behavior arises from the packing demands imposed by the anticuboctahedral ligand polyhedron of $Ru_3(CO)_{12}$.

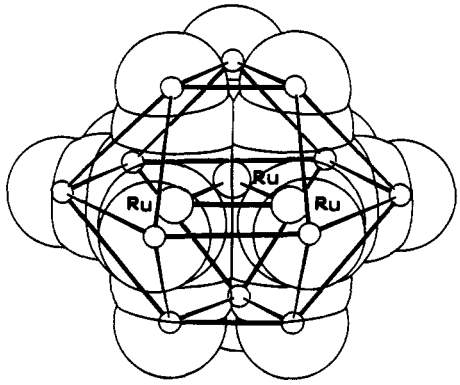

Figure 2. Anticuboctahedral O-atom polyhedron of $Ru_3(CO)_{12}$. The space-filling outline shows the trigonal and tetragonal "clinging" units.

Building a Crystal of $Ru_3(CO)_{12}$. We start from the knowledge of the molecular geometry of $Ru_3(CO)_{12}$ as described by Churchill et al. in 1977.[3] Incidentally, the following discussion applies directly also to the isostructural and isomorphous $Os_3(CO)_{12}$.[11] As we are interested in the *shape* of a $Ru_3(CO)_{12}$ molecule, we can focus our attention on the ligand coverage. The O atom periphery can be connected, as shown in Figure 2, to generate the well-known anticuboctahedral ligand polyhedron. The O atoms are the vertices of two basic structural motifs over the surface: *trigonal units* (either three parallel axial ligands or one axial and two equatorial ones) and *tetragonal units* (two axial and two equatorial ligands). Both these structural motifs can be thought of as "clinging" units to be used by incoming molecules in the crystal-building process.

In the following, we will try to devise a hypothetical crystal-building process, based on these structural motifs. We will first prepare a "one-dimensional" crystal by coupling $Ru_3(CO)_{12}$ molecules, then a "two-dimensional" one, and, eventually, a "three-dimensional" arrangement corresponding to the whole assemblage described above. It must be stressed, however, that the procedure discussed hereafter is only one of the many models that can be conceived to rationalize the variety of intermolecular interactions operating *simultaneously* in a crystal packing.

(i) First Step. Making a Row of Molecules. Our hypothetical crystal-building pathway starts with the recognition that the RM establishes a "key–keyhole" interaction with other two equally oriented molecules, as shown in Figure 3a. It can be seen that, on one side, the RM offers a tetragonal cavity to clasp in an axial ligand of molecule A, while, on the opposite side, it "inserts" an axial CO ligand into a tetragonal cavity of molecule B. This key–keyhole interaction enables us to build up a row

(9) Gavezzotti, A. OPEC, Organic Packing Potential Energy Calculations. University of Milano, Italy, 1987. See also: Gavezzotti, A. *J. Am. Chem. Soc.* **1983**, *95*, 5220.

(10) Keller, E. SCHAKAL88, Graphical Representation of Molecular Models. University of Freiburg, FRG, 1988.

(11) Churchill, M. R.; DeBoer, B. G. *Inorg. Chem.* **1977**, *16*, 878.

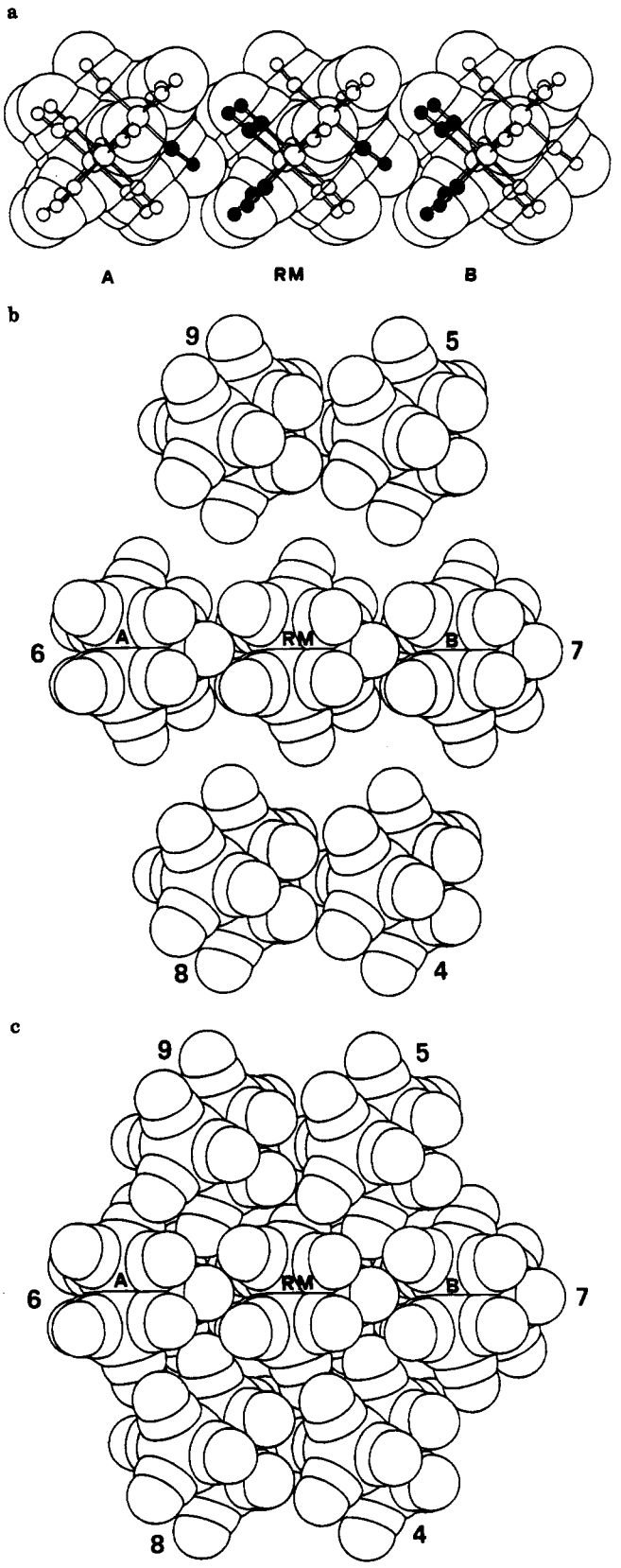

Figure 3. (a) Row of $Ru_3(CO)_{12}$ molecules showing the key–keyhole interaction. Filled atoms evidence the insertion of axial CO's into tetragonal cavities. (b) Adding rows to form a layer via trigonal-to-trigonal and tetragonal-to-tetragonal interlocking. (c) Space-filling projection perpendicular to the plane of molecules 4–9 in Figure 1.

of head-to-tail interacting $Ru_3(CO)_{12}$ molecules.

There are two aspects of this interaction that clearly indicate its relevance in the optimization of the intermo-

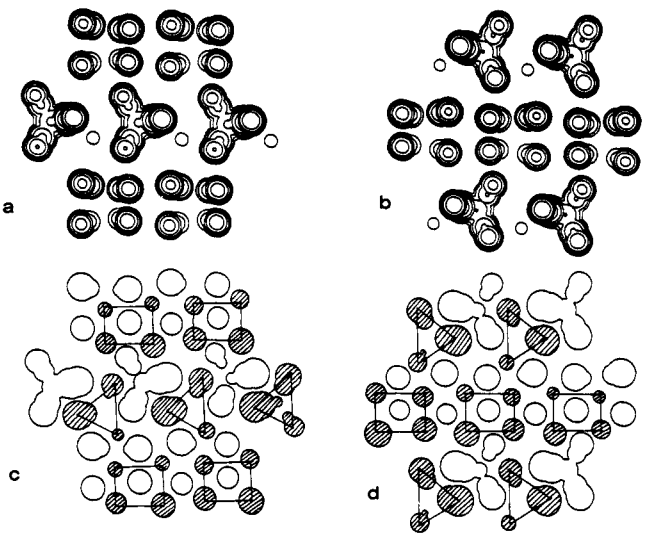

Figure 4. Outermost packing motif above and below the surface of the layer shown in Figure 3c evidenced by incremental grid-cutting from +2 to +4 Å (a) and from −2 to −4 Å (b) (with respect to the plane passing through the centers of mass of the molecules shown in Figure 3b, at 0.2 Å steps (see Figure 3b). (c, d) Grid cut at ±3.7 Å after stacking two new layers above and below. Shaded surfaces refer to atoms belonging to these latter layers.

Chart I

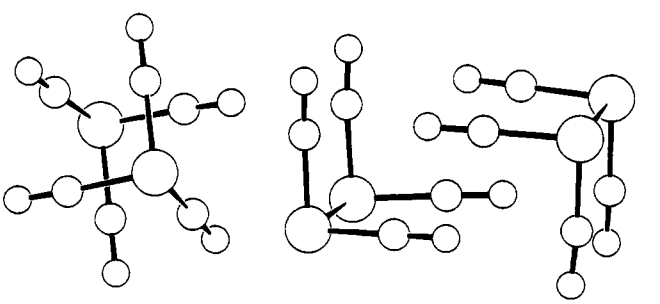

lecular interactions: (i) Among the 12 CO ligands, the locked-in CO group gives the largest individual contribution to the ppe. This can be seen by partitioning the potential energy into the separate CO···CO, CO···Ru, and Ru···Ru contributions, as shown in Table II (see also below). From the value of $\sum_{CO}$, the average contribution $E_{CO} = \sum_{CO}/n_{CO}$ (where $n_{CO} = 12$ in the present case) of a single CO group to the ppe can be calculated. In the case of $Ru_3(CO)_{12}$ such a value is ca. −3.2 kcal mol^{-1}, while the specific contribution of the CO–tetragonal unit interaction is ca. −3.6 kcal mol^{-1}. (ii) There is a clearly identifiable *intramolecular* effect of this interaction. It is well-known that, despite the idealized D_{3h} symmetry, the three Ru–Ru bonds are two "short" and almost identical bonds [2.8521 (4) and 2.8518 (4) Å] and one slightly longer bond [2.8595 (4) Å]. This is the bond corresponding to the key–keyhole interaction. It appears that some Ru–Ru bonding overlap is sacrificed in order to help the widening of the tetragonal cavity accommodating the axial ligand (note that $Os_3(CO)_{12}$ similarly shows one "long" [2.8824 (5) Å] and two "short" bonds [2.8752 (5) and 2.8737 (5) Å]).

(ii) Second Step. Adding Rows To Form a Layer. The molecules of the first row now offer on both sides an alternation of trigonal and tetragonal clinging units. If two identical rows, though in reverted orientations (i.e. molecules related by centers of symmetry), are put side by side (see Figure 3b) with the central one, the trigonal units can interlock along their 3-fold axes, while the tetragonal units can interlock by placing the CO groups as shown in Chart I. The result of this operation is shown in Figure 3c.

Table II. Summary of Crystal and Molecular Qualifiers

species	space group, Z	ppe, kcal mol^{-1}	Σ_{CO}, kcal mol^{-1}	$100\Sigma_{CO}$/ppe	Σ_{CO}/n_{CO}, kcal mol^{-1}	ref
$Ru_3(CO)_{12}$	$P2_1/n$, 4	−67.0	−37.9	56	3.2	3
$Fe_3(CO)_{12}$[a] (Fe as Kr)	$P2_1/n$, 2	−53.7	−36.0	67	3.0	4
$OsFe_2(CO)_{12}$[b]	Pn, 8	−53.5	−36.1	68	3.0	12
$OsFe_2(CO)_{12}$[c]	Pn, 8	−56.8	−36.1	63	3.0	12

[a] Treated in Pn, with $Z = 4$; see text. [b] Both Fe and Os treated as Kr in the ppe calculations. [c] Fe treated as Kr, and Os as Xe in the ppe calculations.

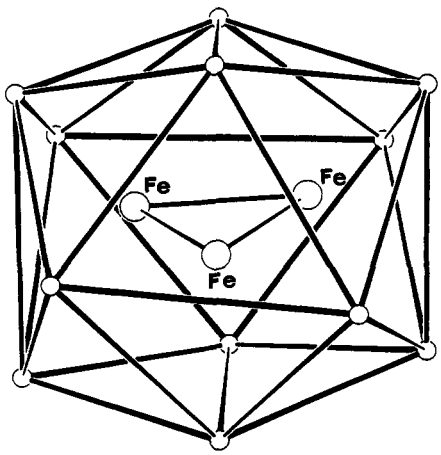

Figure 5. Icosahedral peripheral ligand polyhedron of $Fe_3(CO)_{12}$.

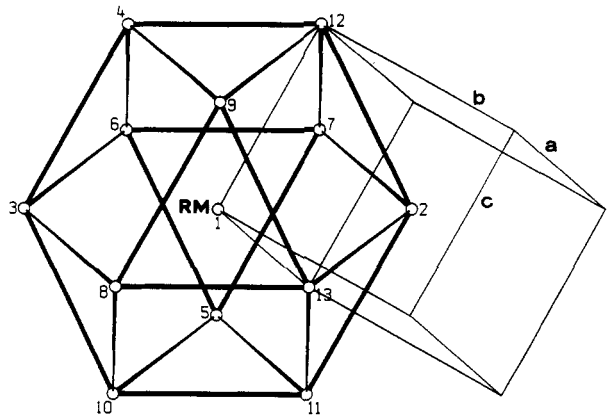

Figure 6. Cuboctahedral ES of $Fe_3(CO)_{12}$ for an ideally ordered distribution of molecules. The unit cell orientation is also shown. Numbers refer to the symmetry operations that generate the packing from the RM. (See caption to Figure 1.)

(iii) Third Step. Adding Layers To Form a Crystal. Parts a and b of Figure 4 show the effect of cutting incremental grids above and below the central layer. This procedure enables us to see that the outermost packing motif above and below the surface of the layer shown in Figure 3c is made up of parallel rows of trigonal and tetragonal units. This is the pattern new layers of molecules will have to cope with in order to generate the stacking sequence seen in Figure 1.

Parts c and d of Figures 4 show the effect of cutting a grid at ±3.7 Å from the origin of the central layer after two new layers of molecules have been added. The shaded surfaces correspond to atoms belonging to these latter layers. It is easy to appreciate that a simple shift allows the parallel CO's of the tetragonal units from above (or below) to penetrate the tetragonal cavities offered by the central layer, while the $(CO)_3$ groups of the trigonal units will have to be inserted between trigonal and tetragonal rows.

Crystal Packing in $Fe_3(CO)_{12}$. The O atoms in $Fe_3(CO)_{12}$ describe a distorted icosahedron (see Figure 5). There are two main differences between the icosahedron and the anticuboctahedron that are relevant for our discussion: (a) an icosahedral polyhedron possesses only triangulated faces, and (b) a regular icosahedron is centrosymmetric, while the anticuboctahedron is not.

The first point implies that only trigonal-to-trigonal (or trigonal-to-digonal, *see below*) interlocking will be possible between $Fe_3(CO)_{12}$ molecules, while the quasi-centrosymmetry implies that the shape of a $Fe_3(CO)_{12}$ molecule will not differ very much if the molecule is in one orientation or its reversed one. This aspect of the icosahedral geometry of the ligand polyhedron in $Fe_3(CO)_{12}$ was recognized in earlier studies and has been invoked to account for the well-known "centrosymmetric" disorder in crystals of $Fe_3(CO)_{12}$. An ideally ordered crystal of $Fe_3(CO)_{12}$ can be described in the space group Pn (noncentrosymmetric subgroup of the actual space group $P2_1/n$), making the molecule distribution around the reference one more readily understandable. The ES obtained for $Fe_3(CO)_{12}$ is depicted in Figure 6 (the symmetry operations and the individual contribution to the ppe are reported as supplementary material). There are 12 molecules that describe a close-packed cuboctahedral ES (thus a piece of ccp arrangement) similar to that found in crystals of $Fe(CO)_5$ and $Mn_2(CO)_{10}$.[1]

The contributions to the ppe (considering the caveat raised above) range from −3.5 to −5.0 kcal mol^{-1} altogether accounting for 93% of the total ppe.

Once again, the hypothetical crystal-building process can begin with the coupling of two molecules and then of a third to make a row.

Let us take the equatorial plane defined by molecules 2, 11, 10, 3, 4, and 12 in Figure 6. A space-filling projection of this plane is shown in Figure 7a. Let us now pick out molecules 2 and 3, which give the highest contribution to the ppe (ca. −5 kcal mol^{-1} each). Their interaction with molecule 1 is based on the interlocking of trigonal units with edges (digonal units) of the central molecule, as shown in Figure 7(b). Molecules 4 and 12 and 10 and 11 are linked to each other in the same way and can now be put on the two sides of the row 3–1–2 to form the layer shown in Figure 7a. The linking will again be based on trigonal-to-trigonal or trigonal-to-digonal interlocking.

Once the layer is made up (but note that, thanks to the symmetry of the ligand envelope, any of the three hexagonal layers can be built in the same way) we can now proceed to add new layers above and below.

Grid-cutting, parallel to the plane, allows a simple identification of the "toothing" patterns. It can be seen from Figure 8 that this pattern is essentially made up of trigonal units having one carbonyl "sticking out" straight from the plane and two CO's roughly parallel to it. Three notably deep (the gridding spans 2 Å) hollow sites are available around the central molecule. These will be used by the molecules of a second layer to push in their trigonal units and yield the cuboctahedral ES seen above.

Disorder and Relationship with $OsFe_2(CO)_{12}$. As mentioned above, the quasi-centrosymmetry of the icosahedral ligand polyhedron brings the molecular orientation and its inverse into near equivalence. This means that the

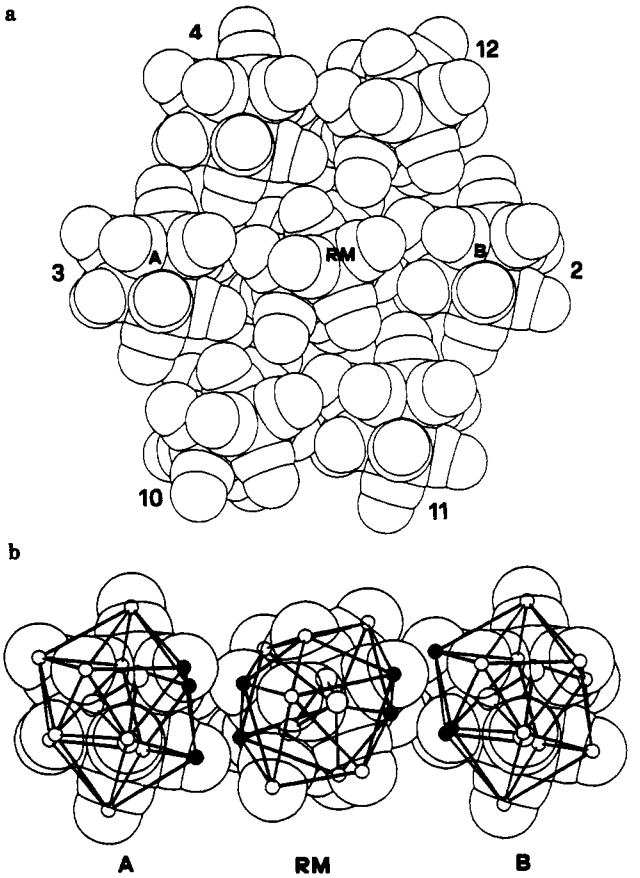

Figure 7. (a) Space-filling projection perpendicular to the hexagonal layers containing molecules 2, 11, 10, 3, 4, and 12 from Figure 6. (b) Trigonal-to-digonal interlocking to form a row of molecules (filled atoms mark the CO ligands involved).

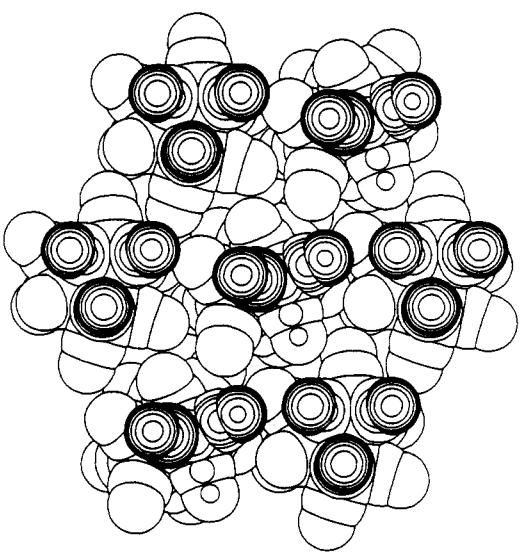

Figure 8. $Fe_3(CO)_{12}$. Grid-cutting between +3 and +5 Å, at 0.2-Å intervals, of the layer shown in Figure 7a, evidencing the CO groups protruding from the surface. The cavities in between are filled with the CO groups of molecules belonging to a second layer.

orientation of the clinging units over the surface of the central layer does not change significantly on replacing the central molecule by a centrosymmetric one. This observation would strengthen the idea that crystals of $Fe_3(CO)_{12}$ *cannot* be ordered, since there is no means for the self-recognition processes to discriminate between these two "identical" outer molecular shapes.

However, similar conclusions would have to be drawn for $OsFe_2(CO)_{12}$,[12] whose outer ligand polyhedron is very similar to, and even more regular than, that of $Fe_3(CO)_{12}$, but the disorder in crystals of $OsFe_2(CO)_{12}$ is only 1:12. The ESs around the two independent molecules in the crystals of this latter species are also of the same kind as for $Fe_3(CO)_{12}$. Thus, if the invariance of the icosahedron to inversion were the true and only reason for $Fe_3(CO)_{12}$ disorder, then $OsFe_2(CO)_{12}$ should also show 1:1 disorder.

This problem has been very clearly laid out by Churchill and Fettinger in their recent paper.[12] These authors have suggested that the disordered structure of $Fe_3(CO)_{12}$ may also result from the twinning of crystalline microdomains in which the individual sites are ordered (or very nearly so) as in $OsFe_2(CO)_{12}$. There is a third hypothesis that can be worth considering (at least for the sake of further speculation on the "saga" of $Fe_3(CO)_{12}$).[13] The possibility of crystal pseudopolymorphism[14] should also be taken into account; i.e., both models are true (this would certainly be most favored by Occham's razor). That is to say that we might be looking at two very close minima of the crystal free energy. In the case of $Fe_3(CO)_{12}$ the entropy gain associated with the disordered structure might counterbalance the potential energy loss caused by the small misfittings in the crystal packing (due to the nonperfect centrosymmetry of the ligand polyhedron). In $OsFe_2(CO)_{12}$, on the other hand, replacing an Fe atom by an Os atom might be sufficient to alter the intermolecular interaction energy in favor of a more ordered distribution of the molecules. [This is reasonable since the percentage contribution of the CO ligands to the crystal potential energy decreases on substituting heavier atoms for Fe (cf. $Ru_3(CO)_{12}$ and $Fe_3(CO)_{12}$ in Table II)]. Although we have no means of simulating the contribution to the ppe of the Os atom in $OsFe_2(CO)_{12}$, it is noteworthy that, if Os is treated as a Ru atom (in which case its contribution is certainly underestimated), the CO···CO contribution to ppe decreases from 68 to ca. 63% (see Table II). Such a treatment strongly suggests that the contribution to the ppe of the inner metal frame is more significant in $OsFe_2(CO)_{12}$ than in $Fe_3(CO)_{12}$ and therefore will be affected by its actual orientation within the CO coverage.

A final comment can be made with respect to the data collected in Table II. As previously noted for the mono- and dinuclear binary carbonyls,[1] the CO groups appear to conform to the homomeric principle;[15] i.e. their average contribution to the ppe (as well as that of any other group of atoms) is fairly constant in any crystal structure irrespective of the molecular geometry. Expectedly, the value of ca. −3 kal mol^{-1} for $\sum_{CO}/n_{CO}$ (with n_{CO} = 12 in our case) falls toward the lower limit of the range observed for the other binary carbonyls (−2.9/−4.0 kcal mol^{-1}),[1] in agreement with the increase of the metal core size on passing from mononuclear to dinuclear, to metal clusters.

Acknowledgment. We thank Prof. B. F. G. Johnson for his careful review of the manuscript and one of the reviewers for some valuable criticisms. Financial support by the Ministero dell'Universitâ e della Ricerca Scientifica e Tecnologica is acknowledged.

Supplementary Material Available: A listing of symmetry operations that generate molecules 2–21 in Figure 1 and 2–13 in Figure 6 (1 page). Ordering information is given on any current masthead page.

(12) Churchill, M. R.; Fettinger, J. C. *Organometallics* **1990**, *9*, 752.
(13) Desiderato, R., Jr.; Dobson, G. R. *J. Chem. Educ.* **1982**, *59*, 752.
(14) Bernstein, J. In *Organic Solid State Chemistry*; Desiraju, G. R., Ed.; Elsevier: Amsterdam, 1987; pp 471–510. Bernstein, J.; Hagler, A. T. *J. Am. Chem. Soc.* **1978**, *100*, 673.
(15) Gavezzotti, A. *J. Am. Chem. Soc.* **1989**, *111*, 1835.